$A=7$, indicating breakdown of the shell model (or only of jj-coupling). These cases were excluded from the least squares fit and were not taken into account in the calculation of the rms deviation. The best values of the coefficients for the various shells are listed in Table II along with the rms deviations. The large difference in the values of a and b between the $p_{1/2}$, $s_{1/2}$ shells and the other shells is not surprising in view of the difference in their meaning in the two cases. It is worth while to note that the deviations in the $d_{5/2}$ shell (and also in the $f_{7/2}$ shell) show a marked regularity. In the middle of the shell all the experimental binding

energies are bigger than those calculated whereas both in the beginning and the end the situation is reversed. This may be associated with the effects of deformation (or possibly of configuration interaction) not considered here. Positions of some excited levels (usually only position of averages) can be calculated with the parameters obtained, and are found to be in fair agreement with the experimental data. It is hoped to report soon on this and related problems. It seems to us that it is interesting and rather surprising that the simple jj-coupling shell model is so adequate in this region of nuclei.

Neutron Scattering from Iron and Carbon by Time-of-Flight*

C. O. Muehlhause, S. D. Bloom, H. E. Wegner,† and G. N. Glasoe
Brookhaven National Laboratory, Upton, New York
(Received April 26, 1956)

A fixed-frequency cyclotron in conjunction with millimicrosecond time-of-flight techniques has been used to study elastic and inelastic neutron scattering from iron and carbon in the Mev range. The elastic angular distribution from iron exhibits an optical diffraction type pattern, and the inelastic angular distribution proves to be primarily isotropic except for a slight asymmetry around 90 degrees. The elastic angular distribution from carbon is in essential agreement with previous work.

INTRODUCTION

THE dynamics of excitation of low-lying nuclear levels is of interest in the study of nuclear structure. Some details of the structure may be investigated by bombarding the nucleus with neutrons and studying the reaction and scattering processes. For most nuclei the energy of the first excited state ranges from ~ 20 kev to ~ 2 Mev. Until recently, identification of various neutron groups from neutron-out reactions in the Mev energy range has been difficult. In the present work this identification was accomplished by determining the flight time for the scattered neutrons over known distances.

Neutrons of 1-Mev energy travel with a velocity of approximately 1.4 cm/mμsec. In order to measure the energy of 1-Mev neutrons to 2% with a flight path of 1 meter, the times of origin and detection must each be known to ~ 1 mμsec. This may be accomplished by using millimicrosecond techniques for scintillation detection together with the short pulse of neutrons obtained from the natural phase bunching of particles accelerated in a fixed-frequency cyclotron.[1] These techniques were applied to the study of elastic and inelastic neutron scattering from iron and carbon.

Elastic and inelastic angular distribution measurements were made for Fe at 1.66, 1.58, and 1.48 Mev, and for C at 1.66 Mev. The elastic distribution exhibits an optical diffraction type pattern, and the inelastic distribution shows a slight asymmetry about 90 degrees.

EXPERIMENTAL PROCEDURE

For this work the 18-in. cyclotron at the Brookhaven National Laboratory produced a 2.45±0.03-Mev external proton beam. About 60 μa of the external beam were focused on a ¼-in. diameter target 12 ft from the cyclotron by using a pair of double-wedge magnets. The natural phase bunching[2] of the machine resulted in a 2-mμsec pulse of protons striking the target every 54.1 mμsec (rf=18.4 Mc/sec).

Neutrons were obtained from a thin target (~ 50 kev) of Zr-T on a water cooled copper backing. Three different primary neutron energies (1.66, 1.58, and 1.48 Mev) were obtained by positioning the scatterer at 0, 20, and 30 degrees with respect to the direction of the protons incident on the target. The target design (see Fig. 1) allowed for very little scattering material in the direction of the forward beam. The targets used showed only a negligible loss of tritium over a 50 000 μa-hr period.

[1] D. Bohm and L. Foldy, Phys. Rev. 72, 649 (1947); B. L. Cohen, Rev. Sci. Instr. 24, 589 (1953).

[2] S. D. Bloom, Phys. Rev. 98, 233 (1955); Bloom, Muehlhause, and Wegner, Phys. Rev. 99, 654 (1955); Bloom, Glasoe, Muehlhause, and Wegner, Phys. Rev. 100, 1248 (1955).

The size of scatterer was determined by a suitable compromise between angular resolution, multiple scattering, and scattered intensity. The iron and carbon samples, each containing 2 moles of material, were in the form of cylinders $\frac{7}{8}$ in. in diameter, $1\frac{1}{2}$ in. long, and were situated 4 in. from the target. Therefore, the angular size of the scatterer resulted in an energy spread of ~ 20 kev in the forward direction. Considering the detector aperture ($\sim 2°$), the target thickness, and the effective size of source and scatterer, there was an over-all energy spread of ~ 75 kev due to the geometry of the system.

The effect of multiple scattering is estimated to be about 5% of the total cross section from the average transmission of about 70% for the samples employed. This effect reduces the angular resolution and increases the apparent inelastic cross section at the expense
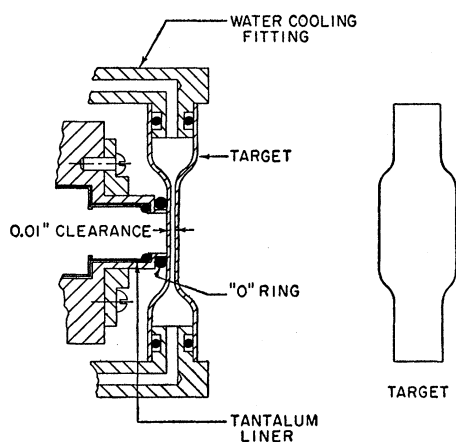

FIG. 1. Zr-T target design.

of the elastic cross section. The angular resolution was $\sim 10°$.

The collimator and shield for the detector, shown in Fig. 2, was composed of a mixture of 500 lb of paraffin and 150 lb of LiF for neutron shielding and 650 lb of Pb for γ-ray shielding. An additional 3 in. of Pb in the nose of the collimator was required for complete suppression of target γ rays. A slightly tapered hole admitted neutrons into the detector. The asymmetrical shape and tapered nose of the collimator provided proper shielding of the detector from direct target neutrons. This design reduced the number of neutrons scattered by the collimator into the detector to a negligible level. The collimator and detector assembly rested upon a steel table constrained to pivot about a point directly below either the target or the scatterer. The flight path indicated is 1.2 m.
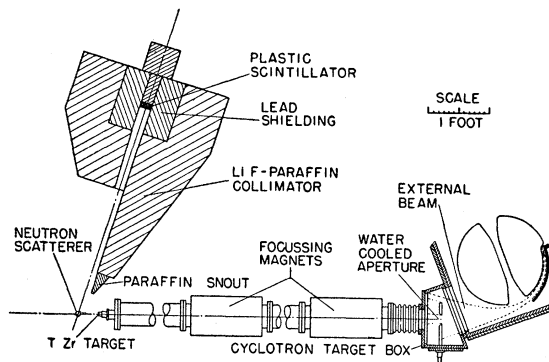
Any fast organic phosphor such as diphenylacetylene

FIG. 2. Plan view of target collimator and detector with scattering sample in position.

or polyvinyltoluene-base plastifluor provided an adequate proton-recoil scintillator. Selected type 1P21 or 5819 photomultiplier tubes were satisfactory. By using two cathode followers, two electronic pulses were obtained from the same event. One of these pulses was used for time analysis (fast pulse); the other was used for pulse height selection (slow pulse).

All fast pulses were mixed with the rf from the cyclotron in a 6218 Philips beam deflection tube[3] (see Fig. 3). This tube is provided with focusing and sweeping electrodes in addition to the usual signal and collector electrodes. By means of a pickup loop near the cyclotron oscillator, 20 v of rf was applied to the sweeping electrodes at some arbitrary phase. The same rf voltage shifted 90° in phase was also applied to the focusing grid, thus permitting charge to appear on the collector
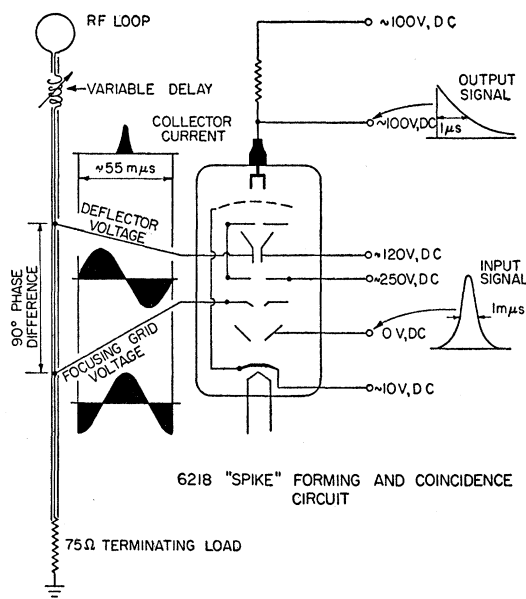

FIG. 3. Schematic diagram of 6218 Philips beam deflection tube.

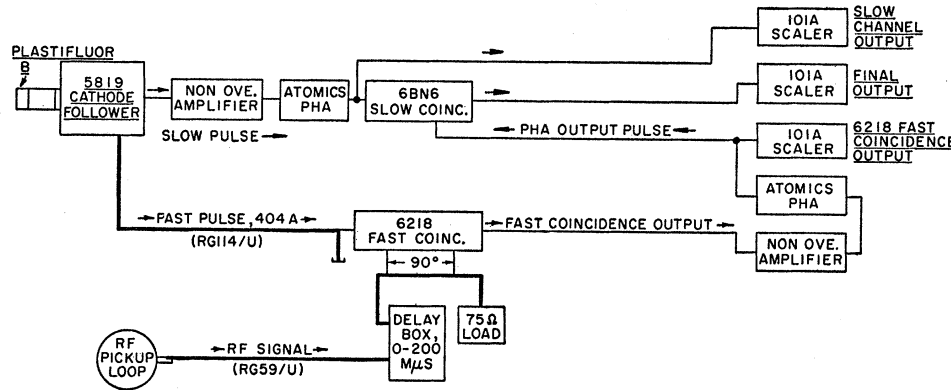[3] Bruysten, Groendijk, and Mantz, Communication News 13, No. 1, 13 (1953).

FIG. 4. Block diagram of detector equipment.

plate only once each rf cycle. An output pulse from the beam tube resulted only when a detector pulse coincided with a null point in the rf wave within the resolving time of the coincidence circuit. This resolving time was determined by the length of a shorted stub on the plate of a 404 A limiting tube.

Pulses in the slow leg of the circuit, after amplification, were selected with a single-channel pulse-height analyzer in order to emphasize proton recoil events. The analyzer output was then mixed with the output of the fast coincidence branch in a slow (5 μsec resolving time) coincidence circuit. Figure 4 shows a block diagram of the electronic equipment.

The time spectrum of the yield from the slow coincidence circuit was obtained by varying the length of the cable conducting the rf signal into the fast coincidence circuit. By varying the length of the shorted stub various channel widths in the time spectrum could be obtained. Both the time resolution and the random-phase background rate were determined by this stub length. The round trip time (τ_{2l}) for electromagnetic waves was determined by measuring the resonance frequency of the stub. The effective time

window (τ_{obs}) was determined by measuring the fraction of random counts, from a radioactive source, passed by the circuit. Table I lists the values of τ_{2l} and τ_{obs} used in this work. The observed systematic difference between τ_{obs} and τ_{2l} indicates that the ultimate time resolution of this coincidence circuit is about 0.2 mμsec.

With the collimator set at 90° with respect to the direction of the primary neutron beam, the time spectrum of the yield was obtained by using the high resolution (HR) stub. A methane proportional counter was used to monitor the neutron intensity from the target. At each time delay, the yield was recorded for

TABLE I. Stub integrals.

Stub	τ_{2l} mμsec	τ_{obs} mμsec
HR	2.38	2.45
γ_i	8.37	8.91
N_e	11.61	12.41
N_i	17.45	18.37

the time $(\sim 60$ sec) required by the monitor to register 10 240 counts. A typical time spectrum for iron is shown in Fig. 5. The identification of the peaks was accomplished by taking similar data with different flight paths. An additional aid in this identification is to allow the direct target γ rays to be displayed in the time spectrum by removing some of the lead in the nose of the collimator.

In Fig. 5 the time zero for neutrons or γ rays leaving the scatterer occurs at 44 mμsec delay. The true time disposition of the scattered radiation is shown in Fig. 6. Note that one rf period has been added to the time differences appearing in Fig. 5.

Having determined the time location of the various peaks, the integrated yield under a particular peak was obtained by using the proper stub $(\gamma_i$ for γ ray, N_e for elastic, and N_i for inelastic), and setting the proper delay. The angular distributions were then obtained by setting the collimator at various angles between 35° and 140°. The γ-ray distribution was measured

FIG. 5. Phase spectrum of 1.66-Mev neutrons scattered at 90° from iron over a 121-cm flight path.

with a higher channel setting in the slow leg in order to exclude the smaller proton recoil pulses.

The elastically scattered neutron intensity at 10° was obtained by the use of a special scatterer assembly shown in Fig. 7. For this measurement the collimator was positioned at 0° and the direct neutron beam was intercepted by the brass fixture. Ring-shaped scatterers of approximately one mole were used.[4] A scattering angle of 10° results from the geometry of the target-scatterer-detector.

The total cross section was determined by measuring a transmission curve for the material under study with the collimator set at 0°.

In order to determine the detector sensitivity as a function of energy the collimator was constrained to pivot about a point under the target. A comparison of the observed angular dependence of neutron intensity with the known angular dependence for the
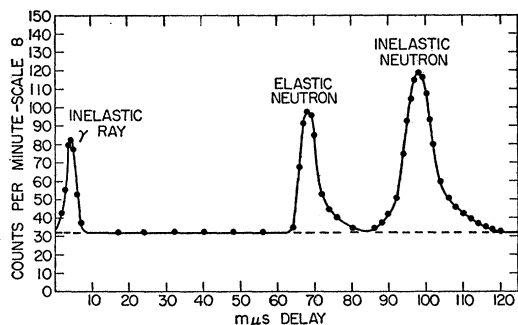

FIG. 6. True time spectrum of 1.66-Mev neutrons scattered from iron at 90° over a 121-cm flight path.
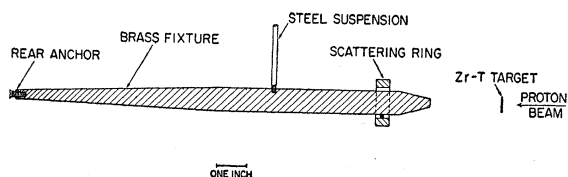

FIG. 7. Schematic diagram of the 10° scattering assembly.

$T(p,n)\mathrm{He}^3$ reaction,[5] yields the desired sensitivity function (see Fig. 8). With the aid of the sensitivity function, the total cross section can be divided into elastic and inelastic components and corrections can be made for the change in neutron energy due to recoil.

The absolute values of the elastic and inelastic components of the total cross sections were determined separately by comparing the total number of elastically scattered neutrons with the total number of neutrons scattered into space. That is, in addition to the aforementioned angular distribution measurements, it was necessary to determine the total number of primary neutrons which the scatterer removed from the beam. The detector was electronically set to integrate over

[4] Darden, Haeberli, and Walton, Phys. Rev. **96**, 836 (1954).

[5] G. Jarvis *et al.*, reported in J. L. Fowler and J. E. Brolley, Revs. Modern Phys. (to be published); see their Fig. 14.
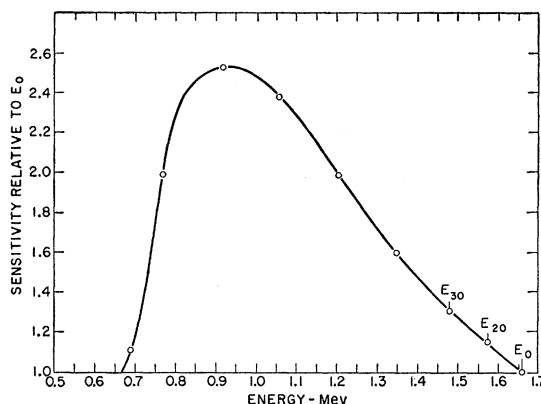
FIG. 8. Neutron detector sensitivity relative to 1.66 Mev. E_0, E_{20}, and E_{30} refer to the three primary energies employed.

the primary peak by using the Ne stub, and the collimator was pivoted about a point under the target for a series of small angles on either side of 0°. The transmission difference for the scatterer was measured over an angular range completely to traverse the sample. Since the scattering sample is not spherical, it was necessary to traverse the sample for a number of different sample orientations. A typical profile is shown in Fig. 9. In this figure, θ' is the angle in the horizontal plane between the collimator direction and the primary beam. The sample orientation about the axis of the beam ($\omega = 45°$ in Fig. 9) is the angle between the major axis of the sample cylinder and the vertical. The normal position of the scatterer was such that the primary beam direction coincided with a minor axis of the cylinder.

The data contained in a complete set of profiles were transformed to the coordinate system corresponding to the normal position of the scatterer. This was done by using the following set of transformation equations:

$$\sin\theta = \sin\theta' \cos\omega,$$
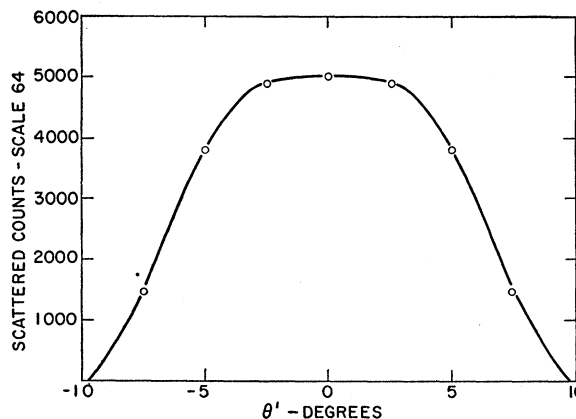$$\cos\phi = \sin\theta' \sin\omega.$$

FIG. 9. Forward zone traverse of iron sample oriented at 45° with respect to the normal and a primary neutron energy 1.58 Mev.
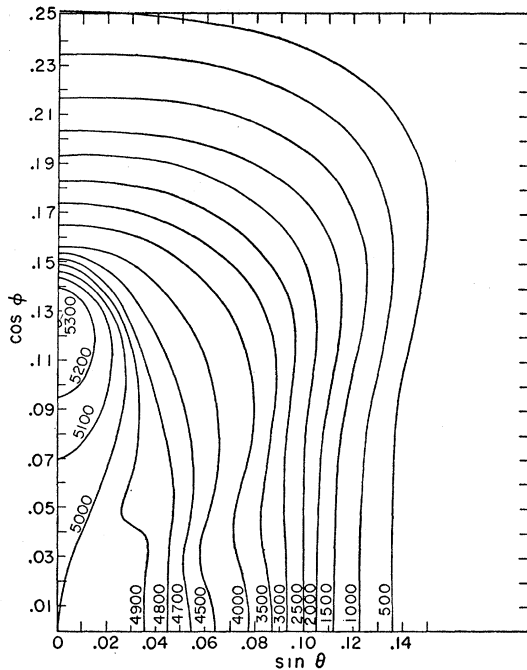
FIG. 10 One quadrant of contour or shadow map for iron at 1.58 Mev. The map is normalized to a central intensity of 64×5000 counts.

Here θ is the angle in the plane of the minor axis measured to the beam direction and ϕ is the azimuthal angle measured to the vertical through the target. The plot of the transformed data yields a shadow or intensity pattern in the forward zone of space, one quadrant of which is given by the contour map of Fig. 10. In this map the central intensity $(\theta=0, \phi=90°)$ was normalized to 5000 counts on a scale of 64.

The integral over this contour map was compared with the integral over the elastic angular distribution
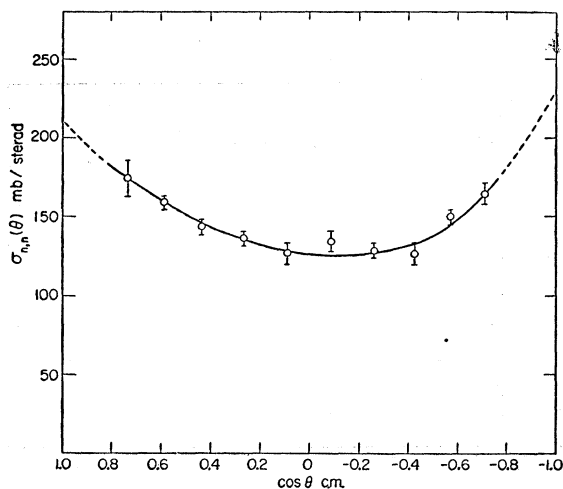

FIG. 11. Angular distribution of 1.66-Mev neutrons elastically scattered from carbon.

to obtain the fraction of the neutrons elastically scattered. Similarly, the integral over the inelastic angular distribution, when corrected for the sensitivity ratio between elastic and inelastic neutrons, gave the number of inelastically scattered neutrons. As before, this was compared with the map integral to obtain the fraction of the neutrons inelastically scattered. The cumulative error resulting from all neutron measurements was indicated by the amount by which the sum of these fractions differed from unity.

An alternative method of cross section calibration is to compare the differential elastic cross section at 10° and the differential inelastic cross section at $\sim 45°$ with the known n-p cross section at these angles. The comparison is made difficult because of the increased time spread of the neutrons scattered from hydrogen.

EXPERIMENTAL RESULTS

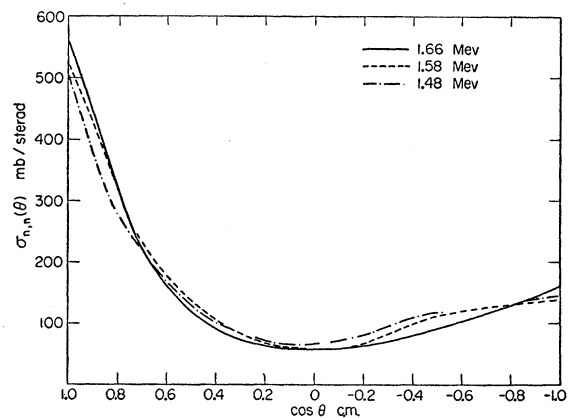The measured differential cross sections in mb/ sterad for Fe and C are shown in Figs. 11–14. The

FIG. 12. Angular distribution of 1.66-, 1.58-, and 1.48-Mev neutrons elastically scattered from iron.

angular distribution is plotted as a function of the cosine of the scattering angle in the center-of-mass system. The distributions were measured in 10° intervals from approximately 30° to 140°. In some cases, a point at 10° was also obtained. Three or four separate runs were made at each energy and the best-fit curve was drawn through the data in each case. The spread in the values obtained is indicated in Figs. 11, 13, and 14, and is typical of all the data.

The angular distribution for the elastic scattering of 1.66-Mev neutrons from C, shown in Fig. 11, was normalized to the measured total cross section of 1.94 b. In all cases the angular distribution data were transformed to the center-of-mass system and were corrected for the change in detector sensitivity which results from the effect of nuclear recoil.

The angular distributions for elastic scattering from iron at 1.66, 1.58, and 1.48 Mev, shown in Fig. 12, were normalized to the elastic cross section at each

energy. The elastic cross sections were determined by multiplying the total cross section by the fraction obtained from the contour map integration as discussed above. The appropriate values for the central intensity are given in Table II. The integrated angular distribution was corrected for the different solid angles subtended by the detector at the scatterer and by the detector at the neutron source. The values for the partial cross sections as well as total cross sections for iron are tabulated in Table II. The difference in the shapes of the angular distributions at the various energies are small and comparable to the uncertainties in the data.

The angular distributions for inelastic scattering from Fe at 1.66 and 1.58 Mev, shown in Fig. 13, were normalized to the inelastic cross sections in the same manner as in the elastic scattering case. An additional correction factor was applied to account for the different sensitivity of the detector for inelastic neutrons.

The errors given in Table II indicate that there is no significant variation in σ_t and σ_e for the three neutron energies. Therefore, the value of σ_i at 1.58 Mev can be interpreted as being too large. Considering this, uncertainty and the errors associated with the points

FIG. 13. Angular distribution of 1.66- and 1.58-Mev neutrons inelastically scattered from iron.

TABLE II. Table of measured iron cross sections.[a]

Mev energy	Scale 64 central intensity	10^{-24} cm^2 σ_e	10^{-24} cm^2 σ_i	10^{-24} cm^2 $\sigma_e + \sigma_i$	10^{-24} cm^2 σ_t
1.66	5050	1.79±0.2	0.95±0.2	2.74±0.3	2.73±0.05
1.58	5120	1.85±0.2	1.27±0.3	3.10±0.4	2.83±0.05
1.48	4245	1.79±0.2	(1.08±0.2)	(2.87±0.05)	2.87±0.05

[a] Values in parentheses were derived from σ_t and σ_e.

of Fig. 13 the two inelastic distributions shown may not be appreciably different. However, both curves do show an asymmetry about 90°.

Since no multiple scattering corrections have been applied to any of the data it is important to indicate the seriousness of this effect. Using the 5% estimate referred to previously, it is evident that about 0.14 b should be subtracted from the inelastic cross sections and the same amount added to the elastic cross sections given in Table II.

The angular distribution of the 845-kev γ ray from Fe^{56*} shown in Fig. 14, was normalized to the neutron data. A symmetry about 90° is indicated.

DISCUSSION

Analysis of the angular distributions for iron given in Figs. 12 and 13 indicate important partial wave contributions from orbital angular momenta up to $l=3$. This is to be expected for neutrons of 1.6-Mev energy ($\lambda=3.6\times10^{-13}$ cm) and the iron radius ($R=5.5\times10^{-13}$ cm). Since the ground state of the predominant isotope of iron (92% Fe^{56}) is 0+, a neutron reaction proceeding through a channel of spin 1/2 could excite
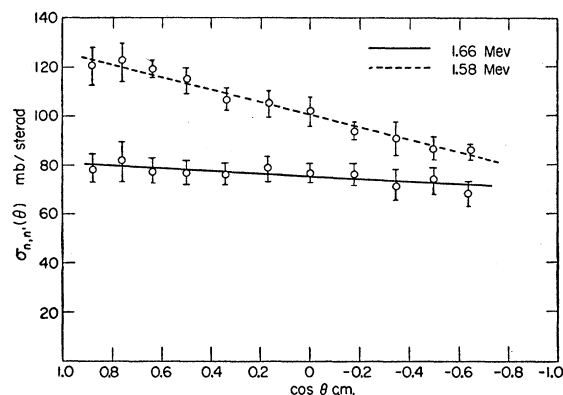
compound nuclear states having any of the following J values: $1/2\pm$, $3/2\pm$, $5/2\pm$, and $7/2-$. The total cross section of iron near 1.6 Mev exhibits a fine structure having fluctuations of about 35%.[6] The level separation as judged in the 100-kev region[7] is ~20 kev. Since the energy spread in the neutron beam employed for this work was about 75 kev, one would not expect to observe large fluctuations with energy (due to compound nucleus formation) in the intensity and shape of the angular distributions. This is consistent with the data obtained.

Excitation of the 845-kev level in iron degrades the initial neutron energy to 700 kev, thereby favoring emergent S and P waves. The inelastic angular distributions shown in Fig. 13 may readily be analyzed into such terms: a large S and a smaller S-P interference term. The precision of the measurements does not justify a more complicated fit, but neither does it imply an exact linear relationship as shown. As discussed in the section on experimental results, the two inelastic angular distributions should not be regarded as different
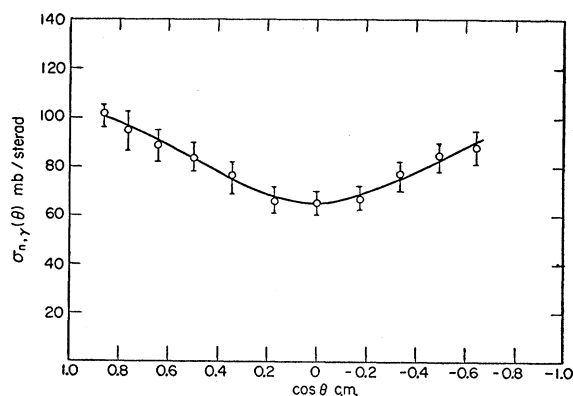

FIG. 14. Angular distribution of 845-kev γ ray from iron for a primary neutron energy of 1.66 Mev.

[6] Barschall, Bockelman, and Seagondollar, Phys. Rev. 73, 659 (1948).

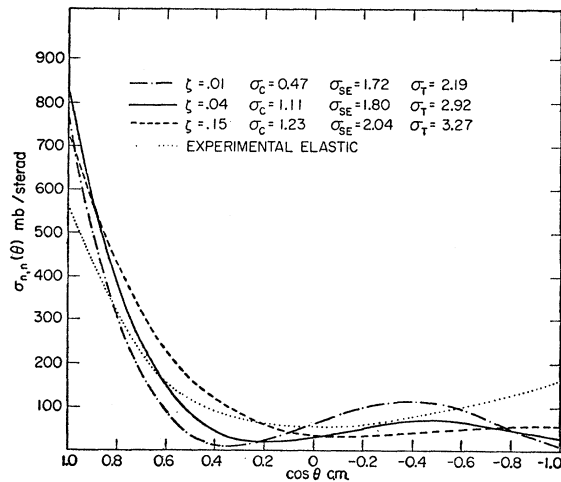[7] Hibdon, Langsdorf, and Holland, Phys. Rev. 85, 595 (1952).

FIG. 15. Calculated shape-elastic angular distribution of 1.66-Mev neutron scattered from iron and experimental elastic angular distribution for 1.66-Mev neutrons scattered from iron.

in magnitude. The asymmetry about 90° of both curves is the most significant feature. This may be regarded as evidence for some direct interaction taking place in the process.[8]

If the excited level in iron is 2+, incoming orbital angular momenta of 2 or 3 are required for a parity allowed reaction. These are in evidence in the elastic angular distributions shown in Fig. 12. A more refined experiment would be required to establish precise correlation between the elastic and inelastic angular distributions.

The diffraction type angular distributions of the elastically scattered neutrons from iron indicate that a comparison with an optical model is in order.[9] The shape-elastic (potential scattering) angular-distributions were calculated for the complex potential:

$$V = -42(1+i\zeta) \text{ Mev}, \quad \zeta = 0.01, 0.04, 0.15,$$

and a primary neutron energy of 1.66 Mev. These are

given in Fig. 15 together with the observed elastic angular distribution at the same energy.

Since $\zeta = 0.15$ corresponds to a mean free path in the nucleus of about 10^{-13} cm this is equivalent to the strong interaction model for nuclear reactions.[10] The general comparison of the experimental results with the curve for $\zeta = 0.15$ is the most favorable. From the calculated cross sections for compound nucleus formation given in the table of Fig. 15 it appears that very little compound elastic scattering is taking place.[11] Most of the nuclear absorption leads to inelastic scattering.

The favoring of large ζ values is in disagreement with the measurements of the average total cross section as a function of energy and atomic weight.[12] However, it is in agreement with the measurements of the inelastic cross section for excitation of the 845-kev γ ray from iron as a function of primary neutron energy, and the measurement of the angular distribution of this γ ray for 1.77-Mev neutron energy ($\zeta = 0.2$).[13]

No special comment regarding the carbon results appears pertinent other than that the data may be fitted by the following expression:

$$d\sigma/d\Omega = A + BP_1 + CP_2,$$

where $B \lesssim 0$.

The time-of-flight technique in conjunction with a fixed-frequency cyclotron eliminates the necessity of beam chopping, provides a high neutron intensity, and has proved to be a useful tool in fast neutron research. At this stage of development, cross sections of ~ 0.1 b can be detected with a neutron energy resolution of ~ 50 kev.

ACKNOWLEDGMENTS

[8] D. M. Brink, Proc. Phys. Soc. (London) **A68**, 994 (1955); S. Hagakawa and S. Yoshida, Proc. Phys. Soc. (London) **A68**, 656 (1955).
[9] Feshbach, Porter, and Weisskopf, Phys. Rev. **96**, 448 (1954).

[10] H. Feshbach and V. F. Weisskopf, Phys. Rev. **76**, 1550 (1949).
[11] The compound elastic scattering cross section is about the same as that involved in multiple scattering, namely 0.14 b.
[12] H. H. Barschall, Phys. Rev. **86**, 431 (1952).
[13] J. J. Van Loef and D. A. Lind, Phys. Rev. **101**, 103 (1956).